Interactions Between Colloidal Knots in Liquid Crystals

Robert W. Eyre and Gareth P. Alexander
Centre for Complexity Science, University of Warwick, Coventry, CV4 7AL, UK

Colloids in nematic liquid crystals interact via the effects of the distortions they create in the director field and the defects formed in response to their existence. Through these interactions, they can chain together to form crystals controllable by external electromagnetic fields. Recent experimental work has lead to the production of colloids in the shape of (p, q) torus knots. We explore the far field effects of such colloids by calculating their dipole and quadrupole moments and find that these have components related to the toroidal and knot geometry that are not present in spherical colloids. Using these dipole and quadrupole moments, we calculate the interaction potential of pairs of links to harmonic order valid at large distances. This lays the grounding for future work considering the interactions of further types of knots, the structures that may be formed from multiple knotted colloids, and what properties these structures possess and what possible uses they may have in areas such as photonics.

I. INTRODUCTION

Knots have always held a place of beauty and fascination in human culture, featuring in the tapestries, mosaics, jewelry, stories, and illustrations of ancient civilisations throughout the world [1]. However, though knots have often been the subject of casual mathematical and scientific thought for centuries, serious quantitative work in knot theory did not begin until the late 1800s [2]. Inspired by the vortex atom model of Lord Kelvin [3], Tait began the first work on the classification of different knots [4]. Since then, knot theory has been established as a significant area of mathematics, and has found many applications throughout science. In the last few decades it has found use in areas such as particle physics [5, 6], quantum computation [7], quantum field theory [8], and the linking and writhing of DNA ribbons [9, 10].

Though knots of any kind are fascinating topological objects, added layers of nontriviality can be found when considering knotted fields. These have been studied in the solutions of classical field theory models [11], the knotting of vortex loops in fluids [12–14], and the knotting of light beams and solutions to Maxwell's equations in electromagnetism [15–17]. One other area of physics where the topology of the system holds great importance and where knots have held great focus in recent years is in liquid crystals.

The properties of nematic liquid crystals are controlled by the defects that form within the material. It has been found that these defects can be manipulated into forming knots in various ways. For instance, by the rewiring and entangling of disclination loops around multiple colloids [18–20]. Colloids themselves, when distributed within a liquid crystal, act like defects and form further defects in response to the surface anchoring conditions of the liquid crystal and the colloid. Knotted colloids have been created experimentally via two-photon photopolymerisation, and have been shown to produce further knotted defects within a liquid crystal dependent on the boundary conditions [21] (see Fig. 1).

The topological properties of liquid crystals have allowed for the creation of novel metamaterials useful in photonics. This can be achieved via the chaining of colloids within a liquid crystal caused by the defects surrounding those colloids [22]. Self-assembling two- and three-dimensional photonic crystals can be formed, controllable by external electromagnetic fields [23–25].

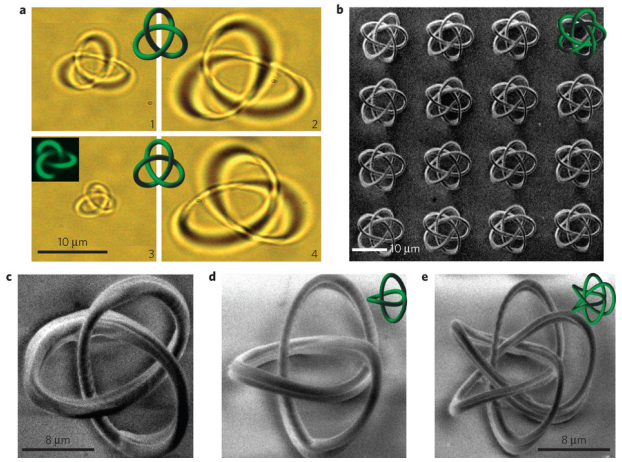

FIG. 1: Examples of knotted colloids from the work of Martinez et al [21]. $(3, 2)$ torus knots in panels **a**, **c**, and **d**. $(5, 3)$ torus knots in panels **b** and **e**.

Following on from this work, and the creation of knotted colloids, we examine the far field interactions of knots in nematic liquid crystals using analogies to multipole moments in electrostatics similar to the work of Lubensky et al [22]. In doing so, we hope to lay the foundation for the formation of interesting structures from knotted colloids within liquid crystals and the exploration of their uses in fields such as photonics.

In section II we provide a brief introduction to the description of defects in liquid crystals. In section III we describe the type of knots we are considering, and how to describe and parameterise them in mathematical terms. In section IV we calculate the dipole and quadrupole mo-

ments of the particular kind of knots we consider, and then in section V we use these multipole moments to calculate approximate far field interactions to harmonic order between pairs of these knots. We then summarise our results in section VI.

II. DEFECTS IN LIQUID CRYSTALS

Liquid crystals are formed from anisotopic molecules, rod-like or disk-like in shape [26]. This anisotropic nature allows liquid crystals to go through various other phases when transitioning from isotropic liquid to fully crystalline solid. The first of these phases is the nematic phase, where the isotropic symmetry is broken resulting in a non-zero average orientation (see Fig. 2). Further phases include the smectic A, smectic C, and cholesteric phases, as well as others, where further symmmetries are broken.

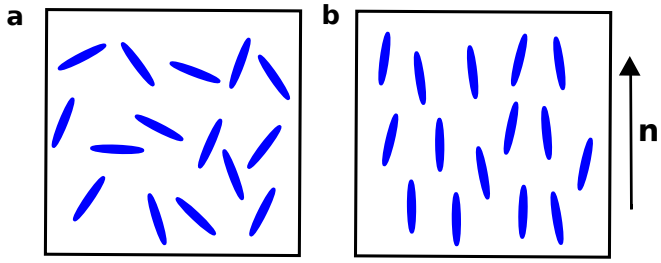

FIG. 2: Arrangement of molecules in isotropic (**a**) and nematic (**b**) liquid crystals. The nematic liquid crystal has a non-zero average orientation described by the director field **n**, which is absent in the isotropic liquid crystal.

We shall focus our work on the nematic phase. The entire system of a nematic liquid crystal can be specified by the director field $\mathbf{n}(\mathbf{r})$, a unit line field which specifies the average orientation at any point $\mathbf{r}$. The director field is formed from a line field due to the indistinguishability of a rod from itself when rotated by π. In other words, $\mathbf{n}(\mathbf{r})$ is indistinguishable from $-\mathbf{n}(\mathbf{r})$.

The energy of the director field is determined by the Frank free energy [26]

$$\begin{aligned} F = & \frac{1}{2}\int d^3r \left\{ K_1 (\nabla\cdot\mathbf{n})^2 + K_2 (\mathbf{n}\cdot\nabla\times\mathbf{n})^2 \right. \\ & + K_3 [\mathbf{n}\times(\nabla\times\mathbf{n})]^2 \\ & \left. - K_{24}\nabla\cdot[\mathbf{n}\times(\nabla\times\mathbf{n}) + \mathbf{n}(\nabla\cdot\mathbf{n})] \right\} . \end{aligned} \quad (1)$$

Each term corresponds to different slowly varying spatial distortions in the director field: the first is splay, the second twist, the third bend, and the fourth saddle-splay. The different K_i are the elastic constants associated with each type of distortion.

What makes the nematic phase interesting is the formation of both point and line defects marking discontinuities in the director field. In two dimensions, we find point defects that can be characterised by the winding number, i.e. the number of times the director field rotates by 2π when taking a circuit around the lone point defect [27]. Due to the indistinguishability of π rotations in the director field, the winding number can take on both integer and half-integer values (see Fig. 3). This can then be extended into three dimensions, where we find point defect "hedgehogs" characterised by an integer topological charge describing the winding of the director field around a surface encompassing the lone defect, and line defect disclinations with half-integer winding around them at any point on the line. These disclinations either stretch from surface to surface in the liquid crystal, or form closed loops. Characterisation of these loops is more complicated than that of a hedgehog [27]. Other such difficulties also exist in the addition of hedgehogs, due to the fact that a $+1$ charge hedgehog can be smoothly deformed into a -1 charge hedgehog [22].

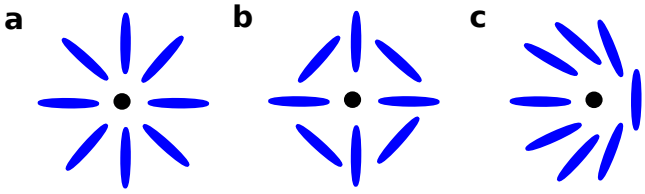

FIG. 3: Winding of the director field around point defects in two dimensions with winding number $+1$ (**a**), -1 (**b**), and $+1/2$ (**c**).

The immersion of colloids into a liquid crystal provides powerful and versatile means of creating and manipulating defects and other topological features in the liquid crystal. The surface anchoring conditions of the colloid enforce that the director field lies normal to the colloid at its surface. For a spherical colloid, this leads to the director pointing radially out at the colloidal surface. For configurations where this is incompatible with the far field director $\mathbf{n}_0$, i.e. when the far field director is uniform, further defects close to the colloid appear. This corresponds to a constraint of zero total topological charge. These defects may take the form of either hyperbolic (-1 topological charge) point defects or disclination loops with $-1/2$ winding at any point on the loop [22]. When such colloids are brought together in the liquid crystal, the defects produced by them allow interactions to occur leading to the chaining of the colloids, for instance with the point defects falling inbetween them.

As knotted colloids can be created experimentally, it is of interest to see what interactions occur when these, rather than spherical colloids, are inserted into the material. Due to the heavily nonlinear nature of the equations involved, we must consider far field approximations like Lubensky et al [22].

III. KNOTS IN LIQUID CRYSTALS

Before we are able to consider far field effects, we need a way to describe our knots. This has been provided by the Milnor construction [28–30].

Consider two complex variables z_1 and z_2 constrained by $|z_1|^2 + |z_2|^2 = 1$. A knot can then be described by the simple polynomial $f(z_1, z_2) = z_1^p + (-iz_2)^q$, since the zeros of this polynomial lie on a (p, q) torus knot (when p and q are coprime) or link (when otherwise) in S^3, see Fig. 4. Knots in R^3 can then be obtained by stereographic projection from S^3. As a standard, we choose the projection point $z_1 = 0$, $z_2 = i$, resulting in the parameterisation of our knot in a cartesian coordinate system of

$$x = \frac{\chi \cos qt}{1 - \sigma \sin(pt + \pi/q)} \tag{2}$$

$$y = \frac{\chi \sin qt}{1 - \sigma \sin(pt + \pi/q)} \tag{3}$$

$$z = \frac{\sigma \cos(pt + \pi/q)}{1 - \sigma \sin(pt + \pi/q)} \tag{4}$$

where $\chi = |z_1|$ and $\sigma = |z_2|$ are related by $\chi^2 + \sigma^2 = 1$ and $\chi^p - \sigma^q = 0$. This parameterisation represents a (p, q) torus knot oriented with its longitude in the x-y plane, and with q-form winding about the longitude, and p-form winding about the meridian, as t varies from 0 to 2π. The positive x axis in relation to t is found where, for $m \in \{0, q-1\}$, $t = 2m\pi/q$. The negative x axis is where $t = (2m+1)\pi/q$. The positive y axis is where $t = (4m+1)\pi/q$. The negative y axis is where $t = (4m+3)\pi/q$. Essentially, the x axis is where the knot begins at $t = 0$. This knowledge will help us in identifying the direction of any multipole moments.

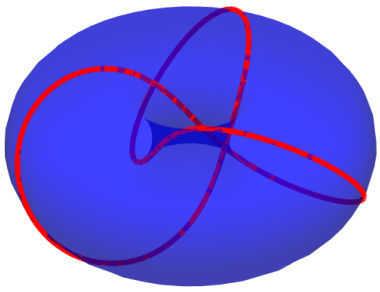

FIG. 4: A $(3, 2)$ torus knot, also known as the trefoil knot.

Note that a different choice of projection point will not affect any results, as it simply leads to rotations of the knot, and switching of p and q. For example, the projection point $z_1 = 1$, $z_2 = 0$ simply gives us a (q, p) torus knot, i.e. with p-form winding about the longitude, and q-form winding about the meridian. A (q, p) torus knot is topologically identical to a (p, q) torus knot [31].

To describe the director field of a knotted liquid crystal defect, we must somehow include winding about the knot. This can be achieved using the argument of the polynomial $\phi = \arg(f(z_1, z_2))$. This winds about the zero line of the polynomial, as constant values of ϕ describe surfaces bounded in some way by the knot (see Fig. 5). Therefore, one possible choice of director field is $\mathbf{n} = (\cos(\phi/2), 0, \sin(\phi/2))$. The factor of $-i$ in front of z_2 in $f(z_1, z_2)$ ensures that ϕ goes to zero far from the knot.

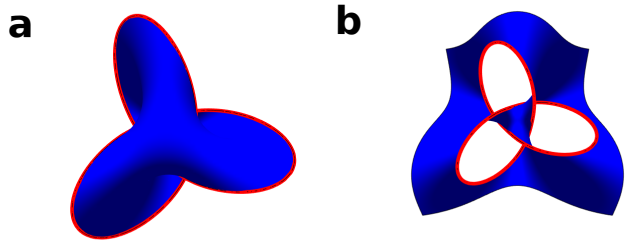

FIG. 5: Constant ϕ surfaces bounded by a trefoil knot, with $\phi = 0$ (**a**) and $\phi = \pi$ (**b**).

With this toolkit, we can now consider the far field effects of knots.

IV. MULTIPOLE MOMENTS OF KNOTS

We have some uniform far field director $\mathbf{n}_0$, and constrain our system such that $\mathbf{n}$ approaches $\mathbf{n}_0$ as $r \to \infty$. In other words, we have zero total topological charge. At large r, we therefore consider small deviations n_μ in $\mathbf{n}$ orthogonal to $\mathbf{n}_0$. Taking the one elastic constant limit, the full nonlinear Frank free energy, equation (1), can be replaced by the harmonic free energy

$$F = \frac{1}{2} K \sum_\mu \int d^3r \, (\nabla n_\mu)^2 \tag{5}$$

which has Euler-Lagrange equation

$$\nabla^2 n_\mu = 0 \ . \tag{6}$$

This is simply the Laplace equation, which at large r has solutions that can be expanded as multipoles. Following Lubensky et al [22], we can calculate these multipole moments for knots, and then consider our knots as approximate point-multipoles. The interactions of these point-multipoles will then be valid at large distances.

As a possible director field is simply a planar field dependent on ϕ, it would seem that the simplest method to find these multipole moments would be to take them

from the far field expansion of ϕ. However, this does not work, as in this case our constraint in (6) reduces to

$$\nabla^2\phi = 0 \ , \tag{7}$$

which is not satisfied.

Another simple method is to just make a direct analogy to electrostatics, where multipole expansions are calculated as standard far field solutions for electric potentials that satisfy Laplace's equation. We must calculate multipole moments for a knotted charge, similar to Werner's work with currents in knotted wires [32] and Lubensky et al [22].

From standard electrostatics [33], we have a scalar function

$$\Phi\left(\mathbf{r}\right) = \frac{1}{4\pi}\int \frac{dq\left(\mathbf{r}'\right)}{\left|\mathbf{r}-\mathbf{r}'\right|} \ . \tag{8}$$

that forms the parts of n_μ that capture the far field effects. $dq\left(\mathbf{r}'\right)$ is an increment of charge distribution representing the winding of the director field about an increment of the knotted curve. For a charge distribution that is localised such that it is only non-vanishing inside some finite sphere around some origin, (8) can be expanded. In rectangular coordinates

$$\Phi\left(\mathbf{r}\right) = \frac{1}{4\pi}\left[\frac{q}{r} + \frac{\mathbf{p}\cdot\mathbf{r}}{r^3} + \frac{1}{2}\sum_{i,j} C_{ij}\frac{x_i x_j}{r^5} + \ldots\right] \ . \tag{9}$$

Here, q is the charge distribution integrated over all space. To ensure that we have zero total topological charge, we require $q = 0$. The dipole moment is given by

$$\mathbf{p} = \int \mathbf{r}'\, dq\left(\mathbf{r}'\right) \ . \tag{10}$$

The quadrupole moment is given by

$$C_{ij} = \int \left(3r'_i r'_j - r'^2\delta_{ij}\right)\, dq\left(\mathbf{r}'\right) \tag{11}$$

where δ_{ij} is the Kronecker delta. We will only consider multipole moments up to the quadrupole moment.

From (2), (3), and (4), we find that the line element of our knot is

$$dl = \frac{\sqrt{\sigma^2 p^2 + \chi^2 q^2}}{1 - \sigma\sin\left(pt + \pi/q\right)}\, dt \ . \tag{12}$$

We have some charge distribution over our knot $\lambda\left(t\right)$, such that $dq\left(\mathbf{r}'\right) = \lambda\left(t\right)\, dt$, which, when integrated over all space, totals to zero. The simplest situation that achieves this is for a special kind of link, corresponding to the case $p = q$. These links are q loops linked together (see Fig. 6). To avoid the loops just overlying each other, we rotate each loop $2\pi/q$ away from the others. We can then attach to each loop some integer or half-integer charge λ_k such that

$$\sum_{k=0}^{q-1}\lambda_k = 0 \ . \tag{13}$$

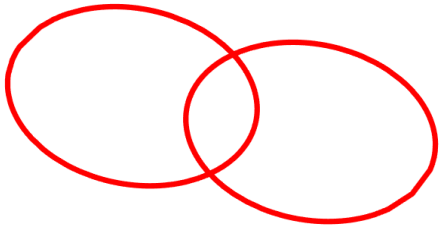

FIG. 6: A $(2,2)$ knot, also known as the Hopf link. Note how one loop is rotated π away from the other.

Taking into account that $p = q$ and therefore $\sigma = \chi = 1/\sqrt{2}$, the dipole moment for a link is then

$$p_x = \sum_{k=0}^{q-1}\frac{\lambda_k}{\sqrt{2}}\int_0^{2\pi}\frac{\cos\left(qt\right)}{\left(1-\frac{1}{\sqrt{2}}\sin\left(qt+\frac{\pi}{q}\left(2k+1\right)\right)\right)^2}\, dt \tag{14}$$

$$p_y = \sum_{k=0}^{q-1}\frac{\lambda_k}{\sqrt{2}}\int_0^{2\pi}\frac{\sin\left(qt\right)}{\left(1-\frac{1}{\sqrt{2}}\sin\left(qt+\frac{\pi}{q}\left(2k+1\right)\right)\right)^2}\, dt \tag{15}$$

$$p_z = \sum_{k=0}^{q-1}\frac{\lambda_k}{\sqrt{2}}\int_0^{2\pi}\frac{\cos\left(qt+\frac{\pi}{q}\left(2k+1\right)\right)}{\left(1-\frac{1}{\sqrt{2}}\sin\left(qt+\frac{\pi}{q}\left(2k+1\right)\right)\right)^2}\, dt \ . \tag{16}$$

The integral in (16) can be very easily solved by substitution, giving $p_z = 0$. The integrals in (14) and (15) can be combined into one integral as $I = p_x + ip_y$. Making the substitution $z = \exp\left(iqt\right)$, this can then be solved using complex contour integration.

The actual dipole moment for a link is found to be

$$p_x = 2\sqrt{2}\pi\sum_{k=0}^{q-1}\lambda_k\sin\left(\frac{\pi\left(2k+1\right)}{q}\right) \tag{17}$$

$$p_y = 2\sqrt{2}\pi\sum_{k=0}^{q-1}\lambda_k\cos\left(\frac{\pi\left(2k+1\right)}{q}\right) \tag{18}$$

$$p_z = 0 \ . \tag{19}$$

Note that opposing charges must be applied to loops that oppose each other in position in order to have a non-zero dipole moment. For even q this corresponds to applying opposing charges to the loops rotated π away from each other. An example of a dipole for a Hopf link can be seen in Fig. 7.

From (11), the various parts of the quadrupole moment tensor can be calculated, and, similar to the dipole moment, all integrals involved can be computed using substitution and complex contour integration.

In order to gain any meaningfulness from the resulting tensor, we must write it in a certain way. The defining geometry of our links is that they rest upon the outside surface of a torus. A torus has a preferred axial direction,

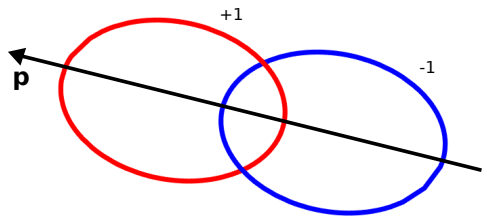

FIG. 7: The dipole for a Hopf link where opposing charges have been assigned to each loop.

orthogonal to the plane which the longitude of the torus sits in (see Fig. 8). We have labelled this direction as the z axis starting at an origin that is situated at the centre of the torus. The torus is invariant under rotations about this direction, i.e. under the rotation subgroup $SO(2)$. As the link is a curve that just happens to sit upon the torus, it is not invariant under this set of rotations. However, it is still natural to decompose the properties of the link into components that transform independently under these rotations.

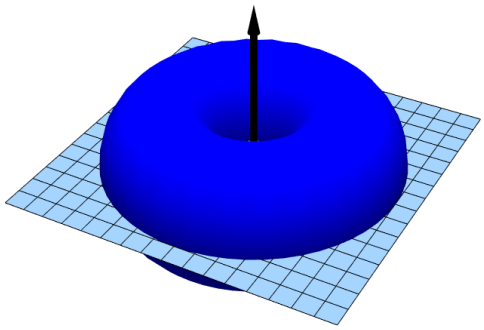

FIG. 8: The geometry of the torus the knot lies on lends itself to the natural splitting of properties into components in the longitudinal plane and in the preferred axial direction.

For the dipole tensor, this involves separating it into one component consisting of a vector in the x-y plane and one consisting of a scalar in the z direction. However, as $p_z = 0$, this second component is zero, and we need not consider it when looking at interactions. For the quadrupole tensor, we separate it out into four components. Two parts are associated with the preferred axial direction. The first is an axial scalar part

$$A_s = \left(5e^{i2\theta_k} - i6\sqrt{2}e^{i\theta_k} - 3\right)\begin{bmatrix}0&0&0\\0&0&0\\0&0&1\end{bmatrix} \tag{20}$$

where we have defined $\theta_k = \pi(2k+1)/q$. The second is an axial vector part

$$A_v = \begin{bmatrix}0&0&6\cos\theta_k\\0&0&-6\sin\theta_k\\6\cos\theta_k&-6\sin\theta_k&0\end{bmatrix} . \tag{21}$$

Two more parts are associated with the plane orthogonal to the preferred axial direction. The first is another scalar part

$$P_s = \left(\left(6\sqrt{2} - i\right)e^{-i\theta_k} + 15\right)\begin{bmatrix}1&0&0\\0&1&0\\0&0&0\end{bmatrix} . \tag{22}$$

The final part is a 2-spin object

$$\begin{aligned} P_{sp} = &-9\cos(2\theta_k)\begin{bmatrix}1&0&0\\0&-1&0\\0&0&0\end{bmatrix} \\ &+6\sin(2\theta_k)\begin{bmatrix}0&1&0\\1&0&0\\0&0&0\end{bmatrix} . \end{aligned} \tag{23}$$

Note, by referring to an object as scalar, vector, or 2-spin, we are referring to the fact that its components transform under the rotations of $SO(2)$ as a scalar, vector, or 2-spin object.

The total quadrupole tensor is then

$$C = \frac{\pi}{\sqrt{2}}\sum_0^{q-1}\lambda_k\left[A_s + A_v + P_s + P_{sp}\right] . \tag{24}$$

This result provides interesting comparisons with the results of Lubensky et al [22]. For the quadrupole set up of a disclination loop around a colloid, we find that the axial vector and 2-spin parts of the quadrupole tensor are equal to zero. As for a link these parts are non-zero, we therefore find that further interactions occur for links that do not occur for simple loops. These are worth looking at in further detail.

As we have only looked at links, the question arises as to how we would repeat this procedure with knots where p and q are coprime. We would need some form of charge distribution over the knot that totals to zero. One possible way is to separate the knot out in to two curves. For instance, for a simple torus we can separate the surface out in to two regions separated by a central line: an inner region of negative charge, and an outer region of equal and opposing positive charge. This can then be approximated as two concentric circles of opposing charge, separated by some small separation that tends

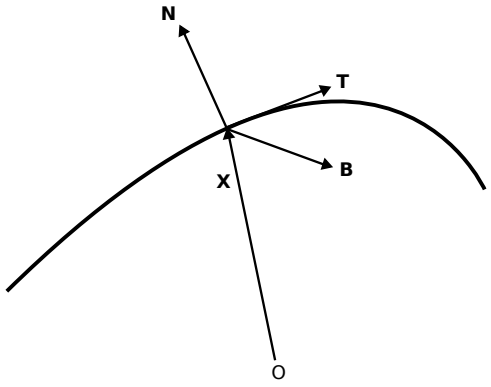

FIG. 9: The basis formed from the tangent vector $\mathbf{T}$, the normal vector $\mathbf{N}$, and the binormal vector $\mathbf{B}$ on a curve $\mathbf{X}$.

to zero whilst the product of the separation and absolute charge value remains finite. This separation from the central line is taken so as to maximise the difference in curvature between the two circles.

As detailed in the review article by Kamien [34], if we consider a curve $\mathbf{X}(s)$ dependent on the arc length s, then the tangent vector to the curve, a unit vector, is given by $\mathbf{T}(s) = \partial_s \mathbf{X}(s)$. From this, we can then define an orthogonal basis of unit vectors that moves around the curve, consisting of the tangent vector $\mathbf{T}(s)$, the unit normal vector $\mathbf{N}(s)$, and the binormal vector $\mathbf{B}(s)$ (see Fig. 9). These vectors are related to each other via the Frenet-Serret equations

$$\partial_s \begin{bmatrix} \mathbf{T}(s) \\ \mathbf{N}(s) \\ \mathbf{B}(s) \end{bmatrix} = \begin{bmatrix} 0 & \kappa(s) & 0 \\ -\kappa(s) & 0 & \tau(s) \\ 0 & -\tau(s) & 0 \end{bmatrix} \begin{bmatrix} \mathbf{T}(s) \\ \mathbf{N}(s) \\ \mathbf{B}(s) \end{bmatrix} \tag{25}$$

where $\kappa(s)$ is the curvature and $\tau(s)$ is the torsion of $\mathbf{X}(s)$. We can therefore consider a curve displaced from $\mathbf{X}(s)$ by a small amount δ

$$\mathbf{X}_\delta(s) = \mathbf{X}(s) + \delta\left(\cos\alpha\,\mathbf{N}(s) + \sin\alpha\,\mathbf{B}(s)\right) \tag{26}$$

that has curvature

$$\kappa_\delta = \left|\frac{ds}{ds_\delta}\right| \left|\partial_s \left(\frac{\partial_s \mathbf{X}_\delta(s)}{|\partial_s \mathbf{X}_\delta(s)|}\right)\right| \tag{27}$$

where s_δ is the arc length of the displaced curve. The value of α required can then be found by maximising κ_δ with respect to α. For the case of a circle, this is found to be $\alpha = 0\,\text{or}\,\pi$, giving the system of concentric circles described. Further work could perform this procedure for the knot parameterisation given in (2), (3), and (4), leading to the calculation of further multipole moments.

V. FAR FIELD INTERACTIONS

Like when calculating the effect of the knot on the director field, the Euler-Lagrange equation for the interactions are highly non-linear. Therefore, we must continue considering far field approximations. We follow Lubensky et al [22] in taking interaction potentials from a constructed phenomenological free energy for two-link interactions where we approximate our links as collections of point-dipoles and point-quadrupoles interacting via pairwise interactions.

First, we note that we make the same assumption as Lubensky et al [22] that the dipole tensor prefers to be alligned with the far field director $\mathbf{n}_0$. Therefore, it is beneficial to rewrite the dipole and quadrupole tensors in a basis with one axis along the dipole moment. Written in terms of our current x, y, z coordinates

$$\mathbf{e}_\alpha = \frac{1}{\rho_q}\sum_{l=0}^{q-1}\begin{bmatrix}\sin(\theta_l)\\ \cos(\theta_l)\\ 0\end{bmatrix} \tag{28}$$

$$\mathbf{e}_\beta = \frac{1}{\rho_q}\sum_{l=0}^{q-1}\begin{bmatrix}-\cos(\theta_l)\\ \sin(\theta_l)\\ 0\end{bmatrix} \tag{29}$$

$$\mathbf{e}_\gamma = \mathbf{e}_z = \begin{bmatrix}0\\0\\1\end{bmatrix} \tag{30}$$

where $\theta_l = \pi(2l+1)/q$ and

$$\rho_q = \left[\left(\sum_{k=0}^{q-1}\lambda_k \sin(\theta_k)\right)^2 + \left(\sum_{k=0}^{q-1}\lambda_k\cos(\theta_k)\right)^2\right]^{1/2}. \tag{31}$$

The dipole tensor is then

$$\tilde{\mathbf{p}} = 2\sqrt{2}\pi\rho_q \mathbf{e}_\alpha \tag{32}$$

and the quadrupole tensor can be written as

$$\tilde{C} = \frac{\pi}{\sqrt{2}}\sum_{k=0}^{q-1}\lambda_k\left[\tilde{A}_s + \tilde{A}_v + \tilde{P}_s + \tilde{P}_{sp}\right] \tag{33}$$

where the scalar parts remain the same, i.e. $\tilde{A}_s = A_s$ and $\tilde{P}_s = P_s$, the vector part is now

$$\tilde{A}_v = \frac{6}{\rho_q}\sum_{l=0}^{q-1}\lambda_l\begin{bmatrix}0 & 0 & \sin(\theta_k+\theta_l)\\ 0 & 0 & \cos(\theta_k+\theta_l)\\ \sin(\theta_k+\theta_l) & \cos(\theta_k+\theta_l) & 0\end{bmatrix}, \tag{34}$$

and the 2-spin object is now

$$\begin{aligned}\tilde{P}_{sp} =& \frac{3}{2\rho_q}\sum_{l=0}^{q-1}\lambda_l\Bigg[\left(\cos(2\theta_k - 2\theta_l)\right.\\ &\left.+5\cos(2\theta_k+2\theta_l)\right)\begin{bmatrix}1&0&0\\0&-1&0\\0&0&0\end{bmatrix}\\ &+\left(\sin(2\theta_k-2\theta_l)\right.\\ &\left.-5\sin(2\theta_k+2\theta_l)\right)\begin{bmatrix}0&1&0\\1&0&0\\0&0&0\end{bmatrix}\Bigg].\end{aligned} \tag{35}$$

We may now consider interactions. We consider a system of dipoles and quadrupoles interacting via pairwise interactions. The dipole- and quadrupole-moment densities are

$$\mathbf{P}(\mathbf{r}) = \sum_{\epsilon} \tilde{\mathbf{p}}^{\epsilon} \delta(\mathbf{r} - \mathbf{r}^{\epsilon}) \tag{36}$$

$$C_{ij}(\mathbf{r}) = \sum_{\epsilon} \tilde{C}^{\epsilon}_{ij} \delta(\mathbf{r} - \mathbf{r}^{\epsilon}) \tag{37}$$

where $\mathbf{r}^{\epsilon}$ is the position of particle ϵ. We can then construct an effective free energy valid at length scales large compared to the link dimensions in the same way as Lubensky et al [22],

$$F = F_{\mathbf{n}} + F_p + F_C + F_{\text{align}} \tag{38}$$

where $F_{\mathbf{n}}$ is the Frank free energy as given by (1), F_p arises from interactions between $\mathbf{P}$ and $\mathbf{n}$, with leading contribution [22]

$$F_p = 4\pi K \int d^3 \left[-\mathbf{P} \cdot \mathbf{n} (\nabla \cdot \mathbf{n}) + \mathbf{P} \cdot (\mathbf{n} \cdot \nabla) \mathbf{n} \right] \ , \tag{39}$$

and F_{align} arises from the alignment of C_{ij} and $\mathbf{n}$

$$F_{\text{align}} = -D \int d^3 r \, C_{ij}(\mathbf{r}) \, n_i(\mathbf{r}) \, n_j(\mathbf{r}) \ . \tag{40}$$

The leading order contribution to the interactions between C_{ij} and $\mathbf{n}$ is

$$F_C = 4\pi K \int d^3 r \, \left[(\nabla \cdot \mathbf{n}) \, \mathbf{n} \cdot \nabla (n_i C_{ij} n_j) - \nabla (n_i C_{ij} n_j) \cdot (\mathbf{n} \cdot \nabla) \mathbf{n} \right] \ . \tag{41}$$

As we shall see, harmonic approximations of this contribution will only include the component of the quadrupole from the dipole direction $\tilde{C}_{\alpha\alpha}$. Further terms that Lubensky et al [22] did not consider could be included that would lead to the inclusion of further parts of the quadrupole tensor such as the axial vector part. Though we do not consider them currently, these possible further terms certainly warrant investigation.

We consider the free energy to harmonic order, where as before we expand to leading order for a small distortion n_μ to the director field in the plane orthogonal to the far field director field $\mathbf{n}_0 = \mathbf{e}_\alpha$, where $\mu = \beta$ or γ. The full effective free energy is then

$$F = K \int d^3 r \, \left[\frac{1}{2} (\nabla n_\mu)^2 - 4\pi P_\alpha \partial_\mu n_\mu + 4\pi (\partial_\alpha C_{\alpha\alpha}) \partial_\mu n_\mu \right] \tag{42}$$

which has Euler-Lagrange equation

$$\nabla^2 n_\mu = 4\pi \partial_\mu \left[P_\alpha(\mathbf{r}) - \partial_\alpha C_{\alpha\alpha}(\mathbf{r}) \right] \tag{43}$$

giving

$$n_\mu(\mathbf{r}) = -\int d^3 r' \, \frac{1}{|\mathbf{r} - \mathbf{r}'|} \partial'_\mu \left[P_\alpha(\mathbf{r}') - \partial'_\mu C_{\alpha\alpha}(\mathbf{r}') \right] \ . \tag{44}$$

Equation (43) determines to leading order at large distances the far field distortions created by a link, as described by the effects of the dipole and quadrupole moments. By using (44) in (42), we can see the effective link-link interactions resulting from this, which, to leading order, are pairwise in nature between the dipole and quadrupole densities

$$\begin{aligned} \frac{F}{4\pi K} = & \frac{1}{2} \int d^3 r \, d^3 r' \, \left[P_\alpha(\mathbf{r}) \, V_{PP}(\mathbf{r} - \mathbf{r}') \, P_\alpha(\mathbf{r}') \right. \\ & + C_{\alpha\alpha}(\mathbf{r}) \, V_{CC}(\mathbf{r} - \mathbf{r}') \, C_{\alpha\alpha}(\mathbf{r}') \\ & \left. + V_{PC}(\mathbf{r} - \mathbf{r}') \left(C_{\alpha\alpha}(\mathbf{r}) \, P_\alpha(\mathbf{r}') - P_\alpha(\mathbf{r}) \, C_{\alpha\alpha}(\mathbf{r}') \right) \right] \ . \end{aligned} \tag{45}$$

With angle ψ between the separation vector $\mathbf{r}$ and the far field director $\mathbf{n}_0$, we find

$$V_{PP}(\mathbf{r}) = \partial_\mu \partial_\mu \frac{1}{r} = \frac{1}{r^3} \left(1 - 3\cos^2 \psi \right) \tag{46}$$

$$V_{CC}(\mathbf{r}) = -\partial_z^2 \partial_\mu \partial_\mu \frac{1}{r} = \frac{1}{r^5} \left(9 - 90\cos^2 \psi + 105\cos^4 \psi \right) \tag{47}$$

$$V_{PC}(\mathbf{r}) = \partial_z \partial_\mu \partial_\mu \frac{1}{r} = \frac{\cos \psi}{r^4} \left(15\cos^2 \psi - 9 \right) \ . \tag{48}$$

From putting (32) and (33) into (45), the interaction energy between a q-link and a p-link separated by some vector $\mathbf{R}$ is given by

$$\begin{aligned} U(\mathbf{R}) = & 4\pi K \left[8\pi^2 \rho_q \rho_p V_{PP}(\mathbf{R}) \right. \\ & + \frac{\pi^2}{2} \sum_{k=0}^{q-1} \sum_{l=0}^{p-1} \lambda_k \lambda_l \left(\tilde{P}^q_{s,\alpha\alpha} + \tilde{P}^q_{sp,\alpha\alpha} \right) \\ & \times \left(\tilde{P}^p_{s,\alpha\alpha} + \tilde{P}^p_{sp,\alpha\alpha} \right) V_{CC}(\mathbf{R}) \\ & + 2\pi^2 \left[\rho_p \sum_{k=0}^{q-1} \lambda_k \left(\tilde{P}^q_{s,\alpha\alpha} + \tilde{P}^q_{sp,\alpha\alpha} \right) \right. \\ & \left. \left. - \rho_q \sum_{l=0}^{p-1} \lambda_l \left(\tilde{P}^p_{s,\alpha\alpha} + \tilde{P}^p_{sp,\alpha\alpha} \right) \right] V_{PC}(\mathbf{R}) \right] \ . \end{aligned} \tag{49}$$

From this potential we can then calculate forces between pairs of links in liquid crystals as a function of separation. Unfortunately, it appears that $\tilde{P}_{sp,\alpha\alpha} = 0$ for any link with a non-zero dipole moment, which requires further investigation. Therefore, we are unable to consider what new interactions the 2-spin and axial vector parts of the quadrupole tensor bring. Further investigations should be made into what further quadrupole interaction terms could be used to explore these new terms.

One of the simplest examples we can consider is that of two Hopf links oriented with their dipole moments along the α axis, with one positioned at some origin, and the other a distance R away at position $(R, 0, 0)$ (see Fig. 10). From (35) and (22) in (49), taking the real part, and differentiating, we can calculate the force between the two Hopf links to be

$$\frac{|\mathbf{F}|}{4\pi K} = -\frac{192\pi^2}{R^4} - \frac{17040\pi^2}{R^6} - \frac{192\pi^2}{R^5} \ . \tag{50}$$

The first term, the dominant one, comes from the dipole-dipole interactions. The second from the quadrupole-quadrupole interactions. The third from the dipole-quadrupole interactions. We find that the force is entirely attractive. There is no repulsive part.

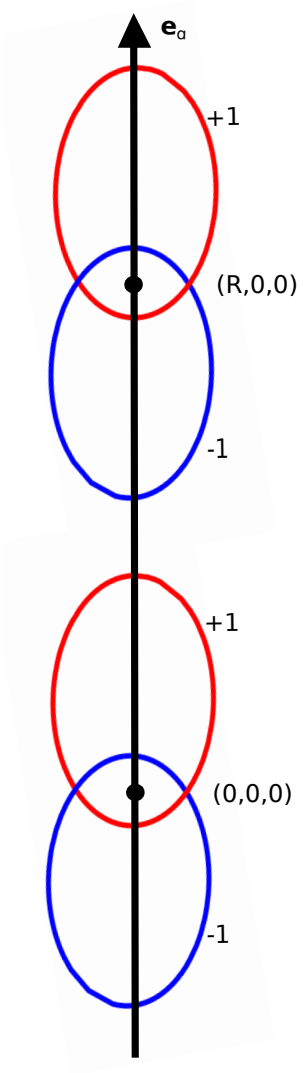

FIG. 10: Example configuration of two Hopf links interacting.

VI. SUMMARY AND CONCLUSIONS

Colloids inserted in nematic liquid crystals lead to the production of defects within the liquid crystal that have been shown both experimentally and theoretically to cause interactions to occur between the colloids. This leads to the chaining of colloids into crystal formations controllable by external electromagnetic fields that are of use in areas such as photonics. Recent experimentation has lead to the production of colloids in the shape of (p, q) torus knots.

In this article, we have combined this recent work in looking at the interactions of (p, q) torus knots in a liquid crystal setting. We have considered harmonic approximations of the interactions in the far field of torus knots with $p = q$, otherwise known as links. We achieved this by calculating both dipole and quadrupole moments for general links. We found that these can be written in the most informative way by considering the toroidal geometry of the situation, thereby splitting the moments into components associated with the longitudinal plane and the preferred axial direction. The dipole moment only has a longitudinal plane component. The quadrupole moment has axial scalar and axial vector components, as well as plane scalar and plane 2-spin components. The values of each component depend on the type of link and the distribution of charge to each loop in the link, i.e. the winding of the director field around each individual loop. The axial vector and plane 2-spin components of the quadrupole moment are zero for colloidal systems considered in the literature. Therefore, these parts have the potential for supplying further interactions that do not occur for simpler colloids.

We calculated pairwise interactions to harmonic order between the dipole and quadrupole moments of multiple links as per Lubensky et al [22]. For the simple example of two Hopf links, we found that the interactions are entirely attractive, and dominated by the dipole-dipole term, suggesting that stable chaining does not occur for this configuration. The extra quadrupole terms that we found do not appear within the interactions we have considered. The axial vector part occurs in further quadrupole terms that we did not consider, that may or may not be able to be included. Our findings imply that the dipole direction component of the 2-spin part is zero for a link with non-zero dipole moment.

Our work lays the foundation for further work into the interactions of knotted colloids. The most obvious work that needs to be done is in finding configurations with a non-zero 2-spin quadrupole component, and in finding further quadrupole interaction terms that involve the axial vector quadrupole component. On doing this, we would then be able to understand the meaning of these terms in the context of the interactions they cause. Multipole moments for (p, q) knots where p and q are coprime could be calculated using the methodology we have built. This will allow for the consideration of interactions of these types of knots, leading to the consideration of the situations found by Martinez et al [21], i.e. knotted colloids with surrounding knotted disclinations.

Overall, this should lead to the investigation of structures formed from multiple knotted colloids, their properties and how we can control them, and their uses in modern materials science.

ACKNOWLEDGMENTS

We thank the Engineering and Physical Sciences Research Council for funding this work. All figures were created using Mathematica and Inkscape, except for Fig. 1 which was reprinted from Martinez et al [21].

[1] S. Jablan, L. Radović, R. Sazdanović, and A. Zeković, Symmetry **4**, 302 (2012).
[2] J. H. Przytycki, Chaos, Solitons & Fractals **9**, 531 (1998).
[3] W. Thomson, Phil. Mag. **34**, 15 (1867).
[4] P. G. Tait, Trans. R. Soc. Edin. **32**, 327 (1884).
[5] L. Brekke, H. Dykstra, S. J. Hughes, and T. D. Imbo, Phys. Lett. B **288**, 273 (1992).
[6] P. Sutcliffe, Proc. R. Soc. A **463**, 3001 (2007).
[7] A. Y. Kitaev, Ann. Phys. **303**, 2 (2003).
[8] E. Witten, Commun. Math. Phys. **121**, 351 (1989).
[9] F. B. Fuller, Proc. Natl. Acad. Sci. USA **75**, 3557 (1978).
[10] R. D. Kamien, Eur. Phys. J. B **1**, 1 (1998).
[11] L. Faddeev and A. J. Niemi, Nature **387**, 58 (1997).
[12] H. K. Moffatt, J. Fluid Mech. **35**, 117 (1969).
[13] X. Liu and R. L. Ricca, J. Phys. A: Math. Theor. **45**, 205501 (2012).
[14] D. Kleckner and W. T. Irvine, Nature Physics **9**, 253 (2013).
[15] A. F. Ranada, J. Phys. A: Math. Gen. **25**, 1621 (1992).
[16] W. T. Irvine and D. Bouwmeester, Nat. Phys. **4**, 716 (2008).
[17] M. R. Dennis, R. P. King, B. Jack, K. O'Holleran, and M. J. Padgett, Nat. Phys. **6**, 118 (2010).
[18] M. Ravnik and S. Žumer, Soft Matter **5**, 269 (2009).
[19] U. Tkalec, M. Ravnik, S. Čopar, S. Žumer, and I. Muševič, Science **333**, 62 (2011).
[20] S. Čopar and S. Žumer, Phys. Rev. Lett. **106**, 177801 (2011).
[21] A. Martinez, M. Ravnik, B. Lucero, R. Visvanathan, S. Žumer, and I. I. Smalyukh, Nat. Mater. **13** (2014).
[22] T. Lubensky, D. Pettey, N. Currier, and H. Stark, Phys. Rev. E **57**, 610 (1998).
[23] I. Muševič, M. Škarabot, U. Tkalec, M. Ravnik, and S. Žumer, Science **313**, 954 (2006).
[24] A. Nych, U. Ognysta, M. Škarabot, M. Ravnik, S. Žumer, and I. Muševič, Nat. Commun. **4**, 1489 (2013).
[25] I. Muševič, Phil. Trans. R. Soc. **371**, 20120266 (2013).
[26] P.-G. De Gennes and J. Prost, *The physics of liquid crystals*, Vol. 23 (Clarendon press Oxford, 1993).
[27] G. P. Alexander, B. G.-g. Chen, E. A. Matsumoto, and R. D. Kamien, Rev. Mod. Phys. **84**, 497 (2012).
[28] J. W. Milnor, *Singular points of complex hypersurfaces*, 61 (Princeton University Press, 1968).
[29] T. Machon and G. P. Alexander, arXiv preprint arXiv:1307.6819(2013).
[30] T. Machon and G. P. Alexander, Phys. Rev. Lett. **113**, 027801 (Jul 2014).
[31] C. C. Adams, *The knot book* (American Mathematical Soc., 1994).
[32] D. H. Werner, in *Antennas and Propagation Society International Symposium, 1997. IEEE., 1997 Digest*, Vol. 2 (IEEE, 1997) pp. 1468–1471.
[33] J. D. Jackson, *Classical electrodynamics*, 3rd ed. (Wiley, 1999).
[34] R. D. Kamien, Rev. Mod. Phys. **74**, 953 (2002).